THE JOURNAL OF PHYSICAL CHEMISTRY LETTERS
A JOURNAL OF THE AMERICAN CHEMICAL SOCIETY

pubs.acs.org/JPCL

Letter

Strong Modulation of Band Gap, Carrier Mobility and Lifetime in Two-Dimensional Black Phosphorene through Acoustic Phonon Excitation

Hongli Guo, Weibin Chu, Oleg V. Prezhdo, Qijing Zheng,* and Jin Zhao

Cite This: *J. Phys. Chem. Lett.* 2021, 12, 3960−3967

Read Online

ACCESS | Metrics & More | Article Recommendations | Supporting Information

ABSTRACT: Black phosphorene (BP) has been attracting intense attention due to its high charge mobility and potential applications in electronic, optical and optoelectronic devices. We demonstrate by *ab initio* molecular dynamics and nonadiabatic quantum dynamics simulations that the excitation of out-of-plane acoustic phonon (ZA) provides strong modulation of the band gap, carrier lifetime and carrier mobility in BP. A 1% tensile strain can significantly enhance ZA mode excitation at room temperature, distinctly reducing the band gap, carrier mobility, and lifetime. These electronic properties can be tuned easily by influencing the excitation amplitude of the ZA mode. Unique to the family of two-dimensional materials, the ZA mode plays an essential role in controlling the electronic properties of BP. The results of our study provide valuable guidelines for design of functional nanodevices based on 2D BP.

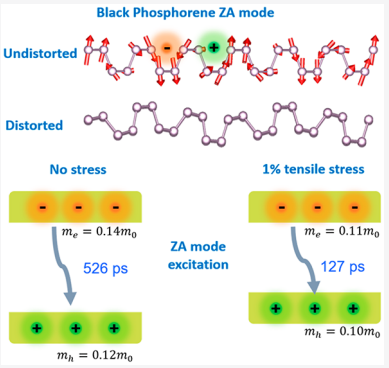

The newly developed two-dimensional (2D) semiconductors have attracted intense interest due to their novel applications in photovoltaics, photocatalysis, and optoelectronics. Among them, the 2D monolayer black phosphorus (BP), also known as black phosphorene, has been attracting intense attention because of its tunable band gap and high carrier mobility.[1−10] In particular, the direct band gap varying from 0.3 eV in bulk to 2.0 eV in monolayer BP enables the absorption of sunlight from ultraviolet to near-infrared in the solar spectrum.[11] The high carrier mobility guarantees its excellent performance in optoelectronic devices.[12−14]

Phonon excitation plays a fundamental role in determining physical properties of 2D materials, including electronic structure, carrier mobility and nonradiative electron−hole (*e-h*) recombination time scale, through the electron−phonon (*e-ph*) coupling. Due to the flexibility and anisotropic puckered geometry, the electronic properties of BP are sensitive to structure distortion. For example, previous studies have shown that external strain can tune the band structure, electrical conductance, optical absorption, and thermal transport.[3,15−19] Such significant effects on the electronic properties due to the geometry distortion suggest that *e-ph* coupling in BP is strong and detailed understanding based on spectroscopic and theoretical studies is beginning to emerge.[20−22] On the experimental side, Mao et al. reported the symmetry dependent *e-ph* coupling in BP by the polarization-selective resonance Raman measurements, focusing on the optical phonon modes.[20] On the theoretical side, Villegas et al. have used many-body perturbation theory to investigate how the *e-ph* coupling induce the band gap opening at increased temperature.[23] Liao et al. studied the effects of *e-ph* coupling on the charge transport and thermoelectric properties.[24] Long et al. and Zhang et al. have provide insights into how the *e-ph* interaction affects the carrier lifetime.[21,22,25] In particular, Zhang et al. propose that the carrier lifetime in defective BP is extended due to excitation of low-frequency phonon modes.[25] All these results suggest that *e-ph* plays an essential role in BP and it is possible to manipulate its electronic properties by phonon excitation.

In this report, we demonstrate using *ab initio* molecular dynamics (AIMD) and nonadiabatic molecular dynamics (NAMD) simulations that the electronic band gap, carrier lifetime and carrier mobility can be modulated effectively by the out-of-plane acoustic phonon mode (ZA) excitation. Comparing with monolayer BP at zero temperature, the band gap is reduced by 90 meV at 300 K due to the *e-ph* coupling between the valence band and the ZA mode. Moreover, it is found that a 1% tensile strain can enhance excitation of the ZA mode distinctly. In this case, the band gap is reduced by 290 meV at 300 K. The enhanced ZA mode excitation also reduces the lifetime of excited carriers. Comparing with monolayer BP without strain, the carrier

Received: March 8, 2021
Accepted: April 14, 2021
Published: April 19, 2021

Downloaded via ZHEJIANG UNIV on April 8, 2026 at 06:50:32 (UTC).
See https://pubs.acs.org/sharingguidelines for options on how to legitimately share published articles.

ACS Publications
© 2021 American Chemical Society

https://doi.org/10.1021/acs.jpclett.1c00747
J. Phys. Chem. Lett. 2021, 12, 3960−3967

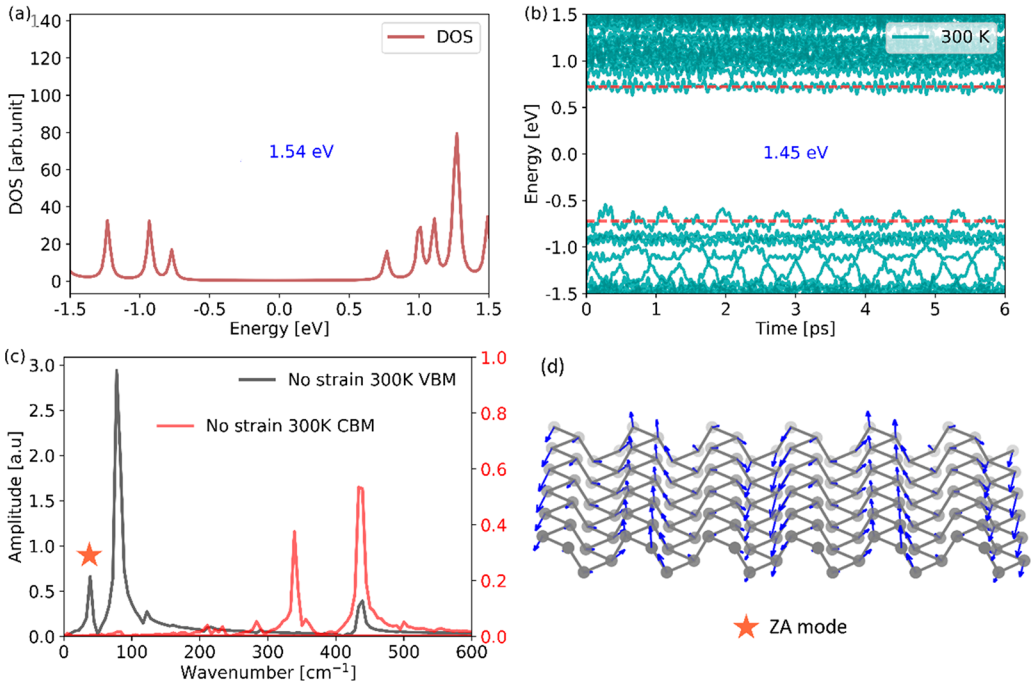

Figure 1. (a) The DOS of the optimized monolayer BP at zero temperature. (b) Evolution of KS energies of monolayer BP at 300 K. Red dash lines reprensent the averaged CBM and VBM energy levels. (c) The FT spectra of the time evolutions of the VBM and CBM at 300 K. (d) Schematic of the ZA phonon mode in monolayer BP.

lifetime is reduced from 526 to 127 ps. Frozen phonon NAMD investigations show that the excited carrier lifetime can be controlled by varying the vibrational amplitude of the ZA mode. Finally, we show that the hole transfer mobility is reduced by 1 order of magnitude due to the strong *e-ph* interaction with the ZA mode. Our study suggests that ZA mode excitation can modulate significantly the electronic band gap, carrier lifetime and mobility in monolayer BP, providing deep insights for future design and customization of functionalities in high-performance 2D electronics and optoelectronics.

There are two categories of *ab initio* methods to investigate the *e-ph* coupling, which are based on statistical sampling or perturbation theory, respectively.[26−33] The sampling methods can be achieved via different ways, for example, Monte Carlo integration or molecular dynamics.[29−33] In this report we use AIMD to investigate the band gap renormalization of BP due to *e-ph* interaction. The AIMD trajectories with length t_0 are used to evaluate the canonical ensemble of energy average as $\langle \epsilon_i^R \rangle_T = \langle \epsilon_i^R \rangle_T^{MD} = \lim_{t_0 \to \infty} \frac{1}{t_0} \int_0^{t_0} \epsilon_i^{R(t)} dt$. Here $\epsilon_i^{R(t)}$ is the energy of the i-th Kohn−Sham eigen-state with the atomic configuration $R(t)$. The nuclei are treat classically, which can draw deviation at low temperature. Yet it is known to be able to achieve reliable results at high temperature.[29] In this report we focus on the BP properties at room temperature and we propose the ensemble based on AIMD is reasonable.

The AIMD is performed using the Vienna *Ab initio* Simulation Package (VASP).[34] The projector augmented wave (PAW)[35] method is used to describe electron−ion interactions and the Perdew−Burke−Ernzerhof (PBE) functional under the generalized gradient approximation (GGA)[36] is used to treat electronic exchange-correlation interactions. We use a 6 × 6 × 1 supercell to model the BP monolayer. A 20 Å vacuum layer in the z-direction is used to eliminate spurious interactions between the periodic images. The relaxed lattice constants along the zigzag and armchair directions are a = 3.31 Å and b = 4.56 Å for the unit cell of the BP monolayer, respectively. For all the considered cases, we choose the plane-wave kinetic energy cutoff of 400 eV, and sample the first Brillouin zone at the Γ point only. All the structures are fully relaxed until the total energy and atomic forces are smaller than 10^{-6} eV and 0.01 eV/Å, respectively. After geometry optimization, the systems are heated to 300 K for 5 ps by velocity rescaling. Then, a 6 ps adiabatic molecular dynamics trajectory is obtained in the microcanonical ensemble (NVE) with a 1 fs atomic time step.

The *ab initio* NAMD simulations used to investigate the carrier lifetimes are carried out using the Hefei-NAMD code[37] within the framework of time-dependent KS theory and classical path approximation.[38,39] Our calculations employ the quantum-classical decoherence induced surface hopping (DISH) scheme for the carrier lifetime investigation.[40−42] The simulation results are based on averaging over 50 different initial configurations and 6000 trajectories sampled for each chosen structure. The 6 ps nonadiabatic (NA) Hamiltonians are iterated 167 times to perform 1 ns NAMD simulation. It is known that the PBE functional underestimates the band gap. Therefore, we have used the hybridized HSE functional[43] to calculate the electronic structure of optimized monolayer BP at zero temperature and used the scissor operator to correct the KS state energies obtained by PBE in the AIMD and NAMD simulation.

The carrier mobility calculations are based on the deformation potential approximation, which has been widely used to calculate the carrier mobility in BP monolayer.[9,16,44,45]

The density of states (DOS) of optimized monolayer BP with the 6 × 6 × 1 supercell is shown in Figure 1a. The band gap obtained by the HSE functional is 1.54 eV, corresponding to the zero temperature without *e-ph* interaction. When the

https://doi.org/10.1021/acs.jpclett.1c00747
J. Phys. Chem. Lett. 2021, 12, 3960−3967

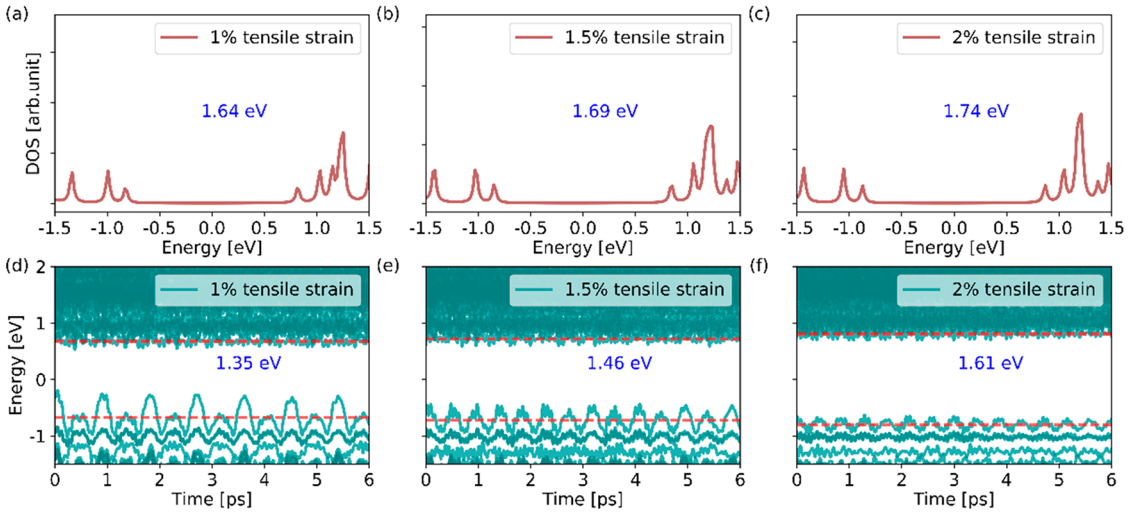

Figure 2. (a−c) The DOS of monolayer BP with 1%, 1.5%, and 2% tensile strain at zero temperature. (d−f) Evolution of KS energies of monolayer BP with 1%, 1.5%, and 2% tensile strain at 300 K. Red dash lines represent the averaged CBM and VBM energy levels.

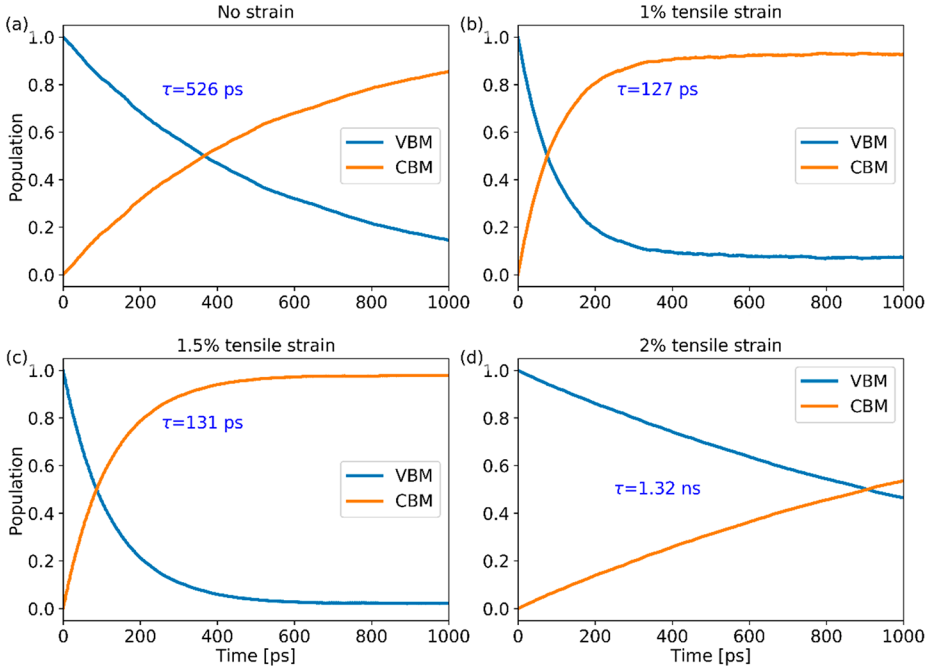

Figure 3. *e-h* recombination dynamics of pristine monolayer BP (a) and monolayer BP under 1% (b), 1.5% (c), and 2% (d) tensile strain.

temperature is increased to 300 K, the *e-ph* interaction can be understood from the time-dependent fluctuations of KS state energies and their Fourier transform (FT) spectra, which are shown in Figure 1b,c. The amplitudes of the energy fluctuations characterize the strength of the *e-ph* interaction, while the FT spectra reveal the dominating phonon mode frequencies contributing to the *e-ph* coupling. The energy level fluctuations indicate that the valence band maximum (VBM) couples with one low-frequency phonon mode with a period around 850 fs, and both VBM and conduction band minimum (CBM) couple with some relatively high-frequency phonon modes with a ∼80 fs period. The FT spectra assigns the high-frequency phonon modes to a major peak around 400 cm^{-1}, which is mainly contributed by the optical out-of-plane A_g^1 mode and the in-plane B_{2g} and A_g^2 modes, similar to the previous report.[25] The low-frequency phonon mode generates the two peaks at 40 and 80 cm^{-1}, with the 80 cm^{-1} peak arising due to the double-frequency effect in the FT. This low-frequency phonon mode is the wave-like out-of-plane acoustic (ZA) mode along the armchair direction (Figure 1d). This mode is unique to the family of 2D materials, and does not appear in 3D systems. As shown in Figure 1b, the energy fluctuation of the VBM due to coupling with the low-frequency ZA mode is as large as 0.3 eV, suggesting a strong *e-ph* coupling. And such, the *e-ph* coupling changes the electronic band gap. At 300 K, the band gap minimum is as small as 1.22 eV and the averaged band gap is 1.45 eV, which is reduced by 90 meV comparing with monolayer BP at 0 K.

The ZA phonon mode, which can reduce the band gap of monolayer BP, is a wave-like acoustic phonon mode along the armchair direction. Naturally, we propose that external strain may affect the ZA mode excitation. We have investigated the monolayer BP with strain from −2% to 2%, in which the negative and positive numbers indicate compressive and tensile

https://doi.org/10.1021/acs.jpclett.1c00747
J. Phys. Chem. Lett. 2021, 12, 3960−3967

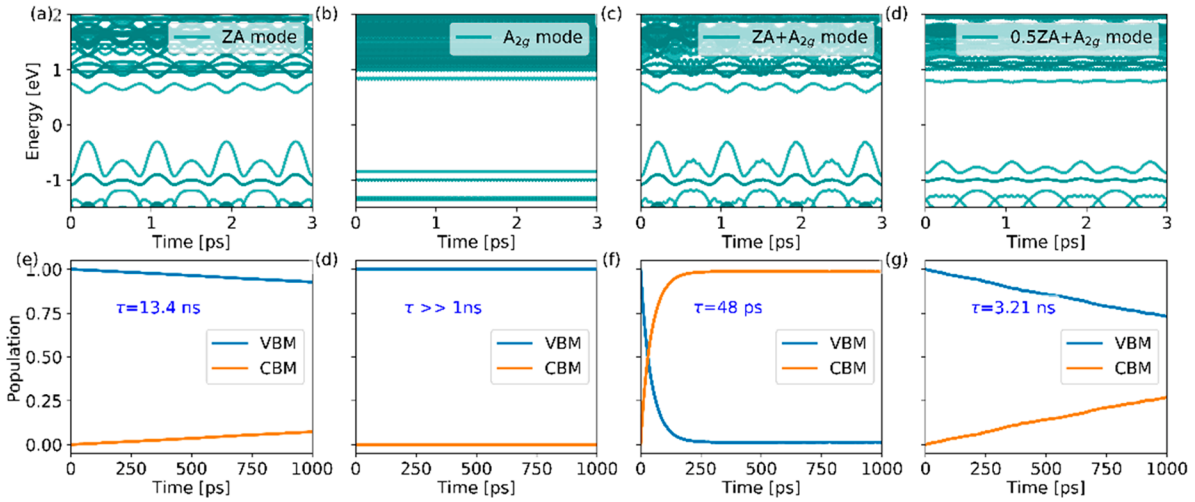

Figure 4. Frozen phonon NAMD simulation of the *e-h* recombination in pristine monolayer BP. (a) The ZA mode is excited with T = 300 K. (b) The A_g^2 mode is excited with T = 300 K. (c) The ZA and A_g^2 modes are excited together with T = 300 K. (d) The ZA mode amplitude is reduced to half, while the A_g^2 mode amplitude is kept the same at T = 300 K.

strain, respectively. Interestingly, we do find that tensile strain affects the ZA mode excitation significantly, while compressive strain has a small effect (see Supporting Information (SI) Figure S1 for more details). Figure 2 shows the DOS of monolayer BP at zero temperature and the time evolution of KS states at 300 K with 1%, 1.5%, and 2% tensile strain. In agreement with previous studies, tensile strain increases the band gap of BP at zero temperature,[15] and for 1% tensile strain, the band gap increases from 1.54 to 1.64 eV. However, 1% tensile strain distinctly enhances the ZA mode excitation at 300 K. The strong *e-ph* coupling of the VBM of monolayer BP with the ZA mode induces energy fluctuation as large as 0.8 eV, and the band gap minimum is as small as 0.84 eV (Figure 2d). The averaged band gap is 1.35 eV. Comparing to zero temperature, the band gap is reduced by 290 meV through the *e-ph* coupling. Importantly, including of the *e-ph* interaction reverses the trend. The band gap is decreased rather than increased if the *e-ph* interaction is taken into account. Further growth of the tensile strain to 1.5% and 2% decreases gradually the ZA mode excitation amplitude. The ZA excitation amplitude at 2% tensile strain is comparable to that in pristine monolayer BP without strain, and the band gap increases to 1.61 eV at 300 K. The *e-ph* coupling still reduces the band gap by 130 meV in this case.

It is noticed the *e-ph* modification on the BP bulk is different with what we find for BP monolayer. In BP bulk, the *e-ph* coupling increases the band gap as shown in SI Figure S2), which is in agreement with previous investigation.[46] It is because in BP bulk both the CBM and VBM are coupled with ZA mode as shown in SI Figure S2(c). In BP monolayer, only the VBM is strongly couple with the ZA mode.

The lifetime of excited carriers (holes and electrons) is determined by the radiative and nonradiative electron−hole recombination time scales. Generally, the radiative electron−hole (*e-h*) recombination is much slower than the nonradiative process,[47] and thus, the nonradiative charge recombination is the dominating factor. The nonradiative charge recombination is determined by the *e-ph* interaction, and we expect the ZA mode excitation to play a significant role. Figure 3 shows the *e-h* recombination dynamics of pristine monolayer BP and monolayer BP with tensile strain obtained using *ab initio* NAMD. Comparing with the pristine BP, the carrier lifetime of monolayer BP with the 1% tensile strain, in which the ZA mode is strongly excited, is reduced by almost four times from 526 to 127 ps. As the tensile strain is increased to 1.5% and 2%, the ZA excitation amplitude is reduced, and the lifetime increases again.

In order to confirm the crucial role of the ZA mode, we use the frozen phonon NAMD to investigate how it affects the *e-h* recombination.[48] Here, we select the ZA mode and one optical A_g^2 mode at 400 cm^{-1} and compare the dynamics of excited carriers in pristine monolayer BP without strain. The vibrational amplitude is obtained from the projection of the AIMD trajectory at 300 K (see SI Figure S3 for more details). First, Figure 4a shows that if only the ZA mode is excited, the *e-h* recombination time scale is as long as 13.4 ns. Similarly, as shown in Figure 4b, if only the A_g^2 mode is excited, we have not observed any *e-h* recombination events within 1 ns, suggesting a long *e-h* recombination time scale beyond what we can achieve in the *ab initio* NAMD simulation. Interestingly, if we excite the ZA and A_g^2 modes together, as shown in Figure 4c, the *e-h* recombination is significantly accelerated and happens within 48 ps. Then, if we reduce the vibrational amplitude of the ZA mode to half of the original amplitude, the *e-h* recombination is again suppressed to the time scale of 3.21 ns (Figure 4d), which is almost 2 orders of magnitude slower. The frozen phonon investigations suggest that the excitation of both ZA and high-frequency optical phonon modes are necessary for the nonradiative *e-h* recombination. Even more interestingly, control of the *e-h* recombination can be realized by tuning the amplitude of the ZA mode. The FT spectra of the time evolutions for band gap of 1%, 1.5% and 2% tensile strained BP are shown in SI Figure S6, demonstrating that the ZA and A_g^2 modes excitation are responsible for the carrier lifetime.

The mechanism of *e-ph* interaction affecting the *e-h* recombination can be understood through the values of the nonadiabatic coupling elements (NACs) and the pure-dephasing time[38] in the frozen-phonon NAMD. Since both CBM and VBM are coupled with the same phonons, their coherence properties are similar, and the decoherence effects play a minor role. The NAC is written as

https://doi.org/10.1021/acs.jpclett.1c00747
J. Phys. Chem. Lett. 2021, 12, 3960−3967

Table 1. Band Gap, *e-h* Recombination Time, Deformation Potential, Effective Mass and Mobility of Excited Electron and Hole in Monolayer BP at Different Strain and Temperature

	band gap (HSE06) (eV)		*e-h* recombination time (ps)	deformation potential (eV)				effective mass (m_e)				mobility ($10^3 cm^2 V^{-1} s^{-1}$)	
	0 K	300 K	300 K	$E^i_{d_y}$		$E^i_{d_ZA}$		0 K		300 K			
				e	h	e	h	e	h	e	h	e	h
no strain	1.54	1.45	526	3.41	−3.51	−8.95	32.75	0.14	0.13	0.14	0.12	0.91	0.08
1%	1.64	1.35	127	2.91	−3.84	−8.82	32.98	0.15	0.14	0.11	0.10	1.45	0.13
1.5%	1.69	1.44	131	3.40	−3.00	−8.97	31.95	0.15	0.14	0.13	0.12	1.19	0.11
2%	1.74	1.61	1320	2.82	−3.72	−9.05	30.92	0.16	0.15	0.14	0.13	1.16	0.11

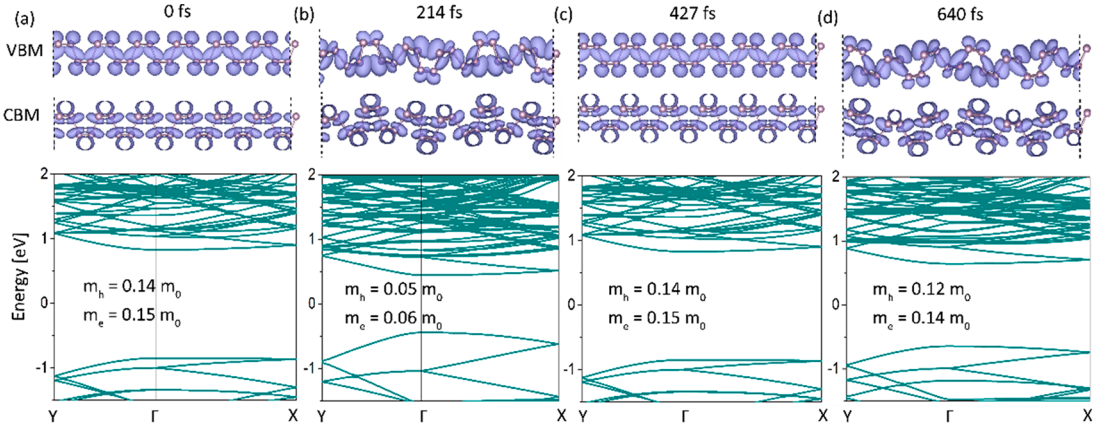

Figure 5. VBM and CBM charge densities and band structures at four snapshots: 0, 214, 427, and 640 fs in monolayer BP. The snapshots at 0 and 427 fs correspond to local minima of the VBM energy with respect to the ZA mode oscillation, and those at 214 and 640 fs are for local maxima. m_h and m_e are effective masses of hole and electron, and m_0 is the effective mass of free electron.

$$d_{jk} = \left\langle \varphi_j \left| \frac{\partial}{\partial t} \right| \varphi_k \right\rangle = \frac{\langle \varphi_j | \nabla_R H | \varphi_k \rangle}{\epsilon_k - \epsilon_j} \dot{R} \quad (1)$$

in which H is the Kohn−Sham Hamiltonian, φ_j, φ_k, ϵ_j, ϵ_k are the corresponding wave functions and eigenvalues for electronic states j and k, and $\dot{R}$ is velocity of the nuclei. The NAC is determined by the *e-ph* coupling elements $\langle \varphi_j | \nabla_R H | \varphi_k \rangle$, energy gap $\epsilon_k - \epsilon_j$ and the nuclear velocity $\dot{R}$. The NACs for the unstrained, 1%, 1.5%, and 2% strained BP are shown in SI Table S1. In the BP system, the coupling with the ZA mode significantly reduces the energy gap between the CBM and the VBM. However, if only the ZA mode is excited, the nuclear velocity is always very low due to the mode's low-frequency. And thus, the *e-h* recombination is very slow in this case. Similar results were also reported for the *e-h* recombination in $MAPbI_3$ recently.[49,50] If the high-frequency optical phonon modes are excited together with the ZA mode, the nuclear velocity will be larger and sufficient to promote the *e-h* recombination. Thus, the ZA and optical phonon modes play different roles in the *e-h* recombination process. The ZA mode is responsible for the reduction of the energy gap, while the high-frequency optical modes contribute the nuclear velocity. Both type of modes contribute to the NACs. The size of the energy gap can be significantly tuned by excitation of the ZA mode, and therefore, the ZA mode excitation can be used to control the rate of the *e-h* recombination.

E-ph interactions also affect the carrier mobility. Using the phonon-limited scattering model, the carrier mobility can be written as[51,52]

$$\mu_{2D} = \frac{e\hbar^3 C_{2D}}{k_B T m^* m_d (E_d^i)^2}$$

where m^* is the effective mass in the transport direction, and m_d is the averaged effective mass determined by $m_d = \sqrt{m_x^* + m_y^*}$. C_{2D} is the elastic modulus of the longitudinal strain in the propagation direction, derived by $(E - E_0)/V_0 = C_{2D}(\Delta l/l_0)^2/2$. E represents the total energy, and V_0 represents the lattice volume at equilibrium for 2D systems. E_d^i is the deformation potential which represents the *e-ph* coupling strength of the ith KS state along the carrier transport direction. In previous investigations, only the longitudinal acoustic phonon mode along the transport direction was considered to calculate the deformation potential. For example, considering carrier transport along the armchair direction (in this manuscript we define it as the y-direction, as shown in Figure 1d), the deformation potential is calculated as $E^i_{d_y} = \Delta V_i/(\Delta l_y/l_0)$. Here, l_0 is the lattice constant, and Δl_y is the change of the lattice constant along the y-direction representing the longitudinal acoustic phonon modes along the y-direction. ΔV_i is the energy change of the ith KS orbital along with the lattice distortion. However, the carrier mobility along the armchair direction is not only affected by the longitudinal acoustic phonon mode in the y-direction, but also influenced by the out-of-plane ZA mode. The deformation potential induced by the ZA mode can be defined similarly as $E^i_{d_ZA} = \Delta V_i/(\Delta l_{ZA}/l_0)$, where Δl_{ZA} is the lattice deformation induced by the ZA mode (see SI Figure S4). We have calculated $E^i_{d_y}$ and $E^i_{d_ZA}$ for the CBM and the VBM, as summarized in Table 1I. The data show that $E^i_{d_ZA}$ is larger than $E^i_{d_y}$ for both the CBM and the VBM. Especially for

https://doi.org/10.1021/acs.jpclett.1c00747
J. Phys. Chem. Lett. 2021, 12, 3960−3967

the VBM, $E^i_{d_ZA}$ is 1 order of magnitude larger due to the strong *e-ph* coupling between the VBM and the ZA mode.

The excitation of the ZA mode not only affects the deformation potential, but also influences the effective mass. Taking BP with the 1% strain as an example, we have calculated the effective mass of the electron and the hole at the CBM and the VBM at four special snapshots at 300 K within one period of the ZA mode. It can be seen that the electron/hole (e/h) effective mass can change from 0.15/0.14 m_e to 0.06/0.05 m_e. The average effective mass at 300 K can be estimated to be 0.11/0.10 m_e. As shown in Figure 5, when the ZA mode is excited, the wave-like geometry enhances the orbital hybridization of the CBM and the VBM, and decreases the effective mass.

Considering both $E^i_{d_y}$ and $E^i_{d_ZA}$, the carrier mobility can be calculated as

$$\mu_{2D} = \frac{e\langle\tau\rangle}{m^*}$$

where $\langle\tau\rangle$ is the averaged relaxation time that can be calculated as

$$\frac{1}{\langle\tau\rangle} = \frac{1}{\tau_y} + \frac{1}{\tau_{ZA}} = \frac{k_B T m_d (E^i_{d_y})^2}{\hbar^3 C_{2D_y}} + \frac{k_B T m_d (E^i_{d_ZA})^2}{\hbar^3 C_{2D_ZA}}$$

in which τ_y and τ_{ZA} represent the relaxation time induced by the longitudinal acoustic phonon in the y-direction and the ZA mode, respectively. Using the averaged effective mass at 300 K, the carrier mobilities along the armchair direction are calculated and shown in Table 1. The hole mobility is reduced significantly due to the large deformation potential of the ZA mode, comparing with the previous studies that did not consider the Z mode. Namely, the hole transport is significantly suppressed by the ZA mode excitation. By contrast, the electron mobility is weakly enhanced due to the increased elastic modulus C_{2D_ZA}.

It is noticed that in the previous AIMD simulations, ZA mode excitation was not discussed. In the paper by Long et al.,[21] there is no significant energy fluctuation for VBM of BP. Zhang et al. have observed the ZA phonon peak,[25] but the intensity of the peak is much lower comparing with the high-frequency phonon peaks. We propose that this is due to the different size of the supercell in the simulation. In this report we use the $6 \times 6 \times 1$ supercell, which is larger than the $5 \times 4 \times 1$ supercell in the work by Zhang et al. We have performed a test simulation using the $1 \times 8 \times 1$ supercell, and the ZA mode is also distinctly excited (Figure S5 in Supporting Information). These results suggest that one needs to employ a sufficiently large supercell along the armchair direction in order to simulate the excitation of the wave-like ZA mode.

The ZA mode is an out-of-plane acoustic phonon representative of the 2D material family. It is distinctly different from the longitudinal and transverse acoustic phonon modes in 3D materials. Therefore, we propose the ZA mode excitation should be sensitive to the environment. For example, interaction between a substrate and monolayer BP should be important for the ZA excitation. In this report, the calculated hole mobility is smaller than in the experimental measurements.[2,12,13] We propose that it is due to existence of the substrate, which may reduce the excitation of the ZA mode.

In our work, it is found that the ZA mode in monolayer BP plays a crucial role to affect the electronic band gap, carrier lifetime and also carrier mobility. Especially, tuning the excitation amplitude of the ZA mode can be used to control these electronic properties. Here we show that external strain can be used to tune the ZA excitation. Besides that, we propose that it is also possible to excite the ZA mode using THz photons at a heterostructure interface, where the out-of-plane interface dipole may help the excitation. It should be noted that for 2D materials like BP, e-h interaction may play an important role in the *e-h* recombination process, our simulations are single-particle based NAMD without taking excitonic effect into account. As discussed in our previous study,[53] when BP is used in practical applications, the *e-h* coulomb interaction will be screened and affected by the substrate or interfacial charge transfer. The excitonic effect may affect the e-h recombination time scale, but the modulation of band gap, carrier lifetime, and mobility through the excitation of ZA mode will not be affected.

In conclusion, using the AIMD and NAMD simulations, we have found that excitation of the out-of-plane ZA mode in BP will affect its electronic band gap, carrier lifetime, and carrier mobility significantly through the *e-ph* coupling. The ZA excitation can be distinctly enhanced with a moderate tensile strain. In the presence of a 1% tensile strain, the band gap of monolayer BP is reduced by 290 meV at 300 K comparing with zero temperature. Comparing with the monolayer BP without strain, the carrier lifetime is reduced from 526 to 127 ps. Frozen phonon NAMD reveals that the carrier lifetime can be controlled by ZA mode excitation. Finally, the carrier mobility is also affected by the ZA mode excitation through increase of the deformation potential and decrease of the effective mass. Our research provides new insights into how the *e-ph* coupling with the ZA mode can be used to influence and customize the electronic properties of 2D monolayer BP, which would be of great interest in the applications of nanodevices.

■ ASSOCIATED CONTENT

Supporting Information

The Supporting Information is available free of charge at https://pubs.acs.org/doi/10.1021/acs.jpclett.1c00747.

Additional information including six figures and one table (PDF)

■ AUTHOR INFORMATION

Corresponding Author

Qijing Zheng − *ICQD/Hefei National Laboratory for Physical Sciences at the Microscale, and CAS Key Laboratory of Strongly-Coupled Quantum Matter Physics, and Department of Physics, University of Science and Technology of China, Hefei, Anhui 230026, China;* orcid.org/0000-0003-0022-3442; Email: zqj@ustc.edu.cn

Authors

Hongli Guo − *ICQD/Hefei National Laboratory for Physical Sciences at the Microscale, and CAS Key Laboratory of Strongly-Coupled Quantum Matter Physics, and Department of Physics, University of Science and Technology of China, Hefei, Anhui 230026, China; School of Physics and Technology, Center for Nanoscience and Nanotechnology, and Key Laboratory of Artificial Micro- and Nano-structures of Ministry of Education, Wuhan University, Wuhan 430072, China*

https://doi.org/10.1021/acs.jpclett.1c00747
J. Phys. Chem. Lett. 2021, 12, 3960−3967

Weibin Chu − *Department of Chemistry, University of Southern California, Los Angeles, California 90089, United States;* orcid.org/0000-0001-5951-0337

Oleg V. Prezhdo − *Department of Chemistry, University of Southern California, Los Angeles, California 90089, United States;* orcid.org/0000-0002-5140-7500

Jin Zhao − *ICQD/Hefei National Laboratory for Physical Sciences at the Microscale, and CAS Key Laboratory of Strongly-Coupled Quantum Matter Physics, and Department of Physics and CAS Center for Excellence in Quantum Information and Quantum Physics, University of Science and Technology of China, Hefei, Anhui 230026, China; Department of Physics and Astronomy, University of Pittsburgh, Pittsburgh, Pennsylvania 15260, United States;* orcid.org/0000-0003-1346-5280

Complete contact information is available at: https://pubs.acs.org/10.1021/acs.jpclett.1c00747

Notes

The authors declare no competing financial interest.

■ ACKNOWLEDGMENTS

J.Z. acknowledges the support of the National Key Foundation of China, Department of Science and Technology, grant nos. 2017YFA0204904, and 2016YFA0200604; the National Natural Science Foundation of China (NSFC), grant no 11620101003,11974322; Anhui Initiative in Quantum Information Technologies (AHY090300). Q.Z. acknowledges the support of the National Natural Science Foundation of China (NSFC), grant no 11704363. O.V.P. acknowledges funding from the U.S. National Science Foundation, grant no. CHE-1900510. H. G acknowledges the funding from China Postdoctoral Science Foundation (Grant No. 2017M622498 and 2018T110789). Calculations were performed, at the Environmental Molecular Sciences Laboratory at the PNNL, a user facility sponsored by the DOE Office of Biological and Environmental Research, Supercomputer Center of Wuhan University and Supercomputing Center at USTC.

■ REFERENCES

(1) Liang, L.; Wang, J.; Lin, W.; Sumpter, B. G.; Meunier, V.; Pan, M. Electronic bandgap and edge reconstruction in phosphorene materials. *Nano Lett.* **2014**, *14* (11), 6400−6406.

(2) Li, L.; Yu, Y.; Ye, G. J.; Ge, Q.; Ou, X.; Wu, H.; Feng, D.; Chen, X. H.; Zhang, Y. Black phosphorus field-effect transistors. *Nat. Nanotechnol.* **2014**, *9* (5), 372.

(3) Zhang, Z.; Li, L.; Horng, J.; Wang, N. Z.; Yang, F.; Yu, Y.; Zhang, Y.; Chen, G.; Watanabe, K.; Taniguchi, T. Strain-modulated bandgap and piezo-resistive effect in black phosphorus field-effect transistors. *Nano Lett.* **2017**, *17* (10), 6097−6103.

(4) Xia, F.; Wang, H.; Jia, Y. Rediscovering black phosphorus as an anisotropic layered material for optoelectronics and electronics. *Nat. Commun.* **2014**, *5*, 4458.

(5) Cai, X.; Mao, L.; Yang, S.; Han, K.; Zhang, J. Ultrafast Charge Separation for Full Solar Spectrum-Activated Photocatalytic H2 Generation in a Black Phosphorus−Au−CdS Heterostructure. *ACS Energy Lett.* **2018**, *3* (4), 932−939.

(6) Buscema, M.; Groenendijk, D. J.; Steele, G. A.; Van Der Zant, H. S.; Castellanos-Gomez, A. Photovoltaic effect in few-layer black phosphorus PN junctions defined by local electrostatic gating. *Nat. Commun.* **2014**, *5*, 4651.

(7) Liu, H.; Neal, A. T.; Zhu, Z.; Luo, Z.; Xu, X.; Tománek, D.; Ye, P. D. Phosphorene: an unexplored 2D semiconductor with a high hole mobility. *ACS Nano* **2014**, *8* (4), 4033−4041.

(8) Warschauer, D. Electrical and optical properties of crystalline black phosphorus. *J. Appl. Phys.* **1963**, *34* (7), 1853−1860.

(9) Qiao, J.; Kong, X.; Hu, Z.-X.; Yang, F.; Ji, W. High-mobility transport anisotropy and linear dichroism in few-layer black phosphorus. *Nat. Commun.* **2014**, *5*, 4475.

(10) Das, S.; Zhang, W.; Demarteau, M.; Hoffmann, A.; Dubey, M.; Roelofs, A. Tunable transport gap in phosphorene. *Nano Lett.* **2014**, *14* (10), 5733−5739.

(11) Castellanos-Gomez, A. Black phosphorus: narrow gap, wide applications. *J. Phys. Chem. Lett.* **2015**, *6* (21), 4280−4291.

(12) Long, G.; Maryenko, D.; Shen, J.; Xu, S.; Hou, J.; Wu, Z.; Wong, W. K.; Han, T.; Lin, J.; Cai, Y. Achieving ultrahigh carrier mobility in two-dimensional hole gas of black phosphorus. *Nano Lett.* **2016**, *16* (12), 7768−7773.

(13) Chen, X.; Wu, Y.; Wu, Z.; Han, Y.; Xu, S.; Wang, L.; Ye, W.; Han, T.; He, Y.; Cai, Y. High-quality sandwiched black phosphorus heterostructure and its quantum oscillations. *Nat. Commun.* **2015**, *6* (1), 1−6.

(14) Yang, S.; Zhang, K.; Ricciardulli, A. G.; Zhang, P.; Liao, Z.; Lohe, M. R.; Zschech, E.; Blom, P. W.; Pisula, W.; Müllen, K. A delamination strategy for thinly layered defect-free high-mobility black phosphorus flakes. *Angew. Chem.* **2018**, *130* (17), 4767−4771.

(15) Rodin, A.; Carvalho, A.; Neto, A. C. Strain-induced gap modification in black phosphorus. *Phys. Rev. Lett.* **2014**, *112* (17), 176801.

(16) Fei, R.; Yang, L. Strain-engineering the anisotropic electrical conductance of few-layer black phosphorus. *Nano Lett.* **2014**, *14* (5), 2884−2889.

(17) Ong, Z.-Y.; Cai, Y.; Zhang, G.; Zhang, Y.-W. Strong thermal transport anisotropy and strain modulation in single-layer phosphorene. *J. Phys. Chem. C* **2014**, *118* (43), 25272−25277.

(18) Quereda, J.; San-Jose, P.; Parente, V.; Vaquero-Garzon, L.; Molina-Mendoza, A. J.; Agraït, N.; Rubio-Bollinger, G.; Guinea, F.; Roldán, R.; Castellanos-Gomez, A. Strong modulation of optical properties in black phosphorus through strain-engineered rippling. *Nano Lett.* **2016**, *16* (5), 2931−2937.

(19) Huang, S.; Zhang, G.; Fan, F.; Song, C.; Wang, F.; Xing, Q.; Wang, C.; Wu, H.; Yan, H. Strain-tunable van der Waals interactions in few-layer black phosphorus. *Nat. Commun.* **2019**, *10* (1), 1−7.

(20) Mao, N.; Tang, J.; Xie, L.; Wu, J.; Han, B.; Lin, J.; Deng, S.; Ji, W.; Xu, H.; Liu, K. Optical anisotropy of black phosphorus in the visible regime. *J. Am. Chem. Soc.* **2016**, *138* (1), 300−305.

(21) Long, R.; Fang, W.; Akimov, A. V. Nonradiative electron−hole recombination rate is greatly reduced by defects in monolayer black phosphorus: *ab initio* time domain study. *J. Phys. Chem. Lett.* **2016**, *7* (4), 653−659.

(22) Zhang, L.; Vasenko, A. S.; Zhao, J.; Prezhdo, O. V. Monoelemental properties of 2D black phosphorus ensure extended charge carrier lifetimes under oxidation: time-domain *ab initio* analysis. *J. Phys. Chem. Lett.* **2019**, *10* (5), 1083−1091.

(23) Villegas, C. E. P.; Rocha, A. R.; Marini, A. Anomalous Temperature Dependence of the Band Gap in Black Phosphorus. *Nano Lett.* **2016**, *16* (8), 5095−5101.

(24) Liao, B.; Zhou, J.; Qiu, B.; Dresselhaus, M. S.; Chen, G. Ab initio study of electron-phonon interaction in phosphorene. *Phys. Rev. B: Condens. Matter Mater. Phys.* **2015**, *91* (23), 235419.

(25) Zhang, L.; Chu, W.; Zheng, Q.; Benderskii, A. V.; Prezhdo, O. V.; Zhao, J. Suppression of Electron−Hole Recombination by Intrinsic Defects in 2D Monoelemental Material. *J. Phys. Chem. Lett.* **2019**, *10* (20), 6151−6158.

(26) Giustino, F. Electron-phonon interactions from first principles. *Rev. Mod. Phys.* **2017**, *89* (1), 015003.

(27) Yildirim, T.; Gülseren, O.; Lynn, J. W.; Brown, C. M.; Udovic, T. J.; Huang, Q.; Rogado, N.; Regan, K. A.; Hayward, M. A.; Slusky, J. S.; He, T.; Haas, M. K.; Khalifah, P.; Inumaru, K.; Cava, R. J. Giant Anharmonicity and Nonlinear Electron-Phonon Coupling in MgB2: A Combined First-Principles Calculation and Neutron Scattering Study. *Phys. Rev. Lett.* **2001**, *87* (3), 037001.

(28) Agapito, L. A.; Bernardi, M. *Ab initio* electron-phonon interactions using atomic orbital wave functions. *Phys. Rev. B: Condens. Matter Mater. Phys.* **2018**, *97* (23), 235146.
(29) Zacharias, M.; Scheffler, M.; Carbogno, C. Fully anharmonic nonperturbative theory of vibronically renormalized electronic band structures. *Phys. Rev. B: Condens. Matter Mater. Phys.* **2020**, *102* (4), 045126.
(30) Monserrat, B.; Drummond, N. D.; Pickard, C. J.; Needs, R. J. Electron-Phonon Coupling and the Metallization of Solid Helium at Terapascal Pressures. *Phys. Rev. Lett.* **2014**, *112* (5), 055504.
(31) Patrick, C. E.; Giustino, F. Quantum nuclear dynamics in the photophysics of diamondoids. *Nat. Commun.* **2013**, *4* (1), 2006.
(32) Lahnsteiner, J.; Kresse, G.; Kumar, A.; Sarma, D. D.; Franchini, C.; Bokdam, M. Room-temperature dynamic correlation between methylammonium molecules in lead-iodine based perovskites: An ab initio molecular dynamics perspective. *Phys. Rev. B: Condens. Matter Mater. Phys.* **2016**, *94* (21), 214114.
(33) Pan, D.; Wan, Q.; Galli, G. The refractive index and electronic gap of water and ice increase with increasing pressure. *Nat. Commun.* **2014**, *5* (1), 3919.
(34) Kresse, G.; Furthmüller, J. Efficient iterative schemes forab initiototal-energy calculations using a plane-wave basis set. *Phys. Rev. B: Condens. Matter Mater. Phys.* **1996**, *54* (16), 11169−11186.
(35) Blöchl, P. E. Projector augmented-wave method. *Phys. Rev. B: Condens. Matter Mater. Phys.* **1994**, *50* (24), 17953−17979.
(36) Perdew, J. P.; Burke, K.; Ernzerhof, M. Generalized Gradient Approximation Made Simple. *Phys. Rev. Lett.* **1996**, *77* (18), 3865−3868.
(37) Zheng, Q.; Chu, W.; Zhao, C.; Zhang, L.; Guo, H.; Wang, Y.; Jiang, X.; Zhao, J. *Ab initio* nonadiabatic molecular dynamics investigations on the excited carriers in condensed matter systems. *Wiley Interdiscip. Rev.: Comput. Mol. Sci.* **2019**, *9* (6), e1411.
(38) Akimov, A. V.; Prezhdo, O. V. The PYXAID program for non-adiabatic molecular dynamics in condensed matter systems. *J. Chem. Theory Comput.* **2013**, *9* (11), 4959−4972.
(39) Akimov, A. V.; Prezhdo, O. V. Advanced capabilities of the PYXAID program: integration schemes, decoherence effects, multi-excitonic states, and field-matter interaction. *J. Chem. Theory Comput.* **2014**, *10* (2), 789−804.
(40) Craig, C. F.; Duncan, W. R.; Prezhdo, O. V. Trajectory surface hopping in the time-dependent Kohn-Sham approach for electron-nuclear dynamics. *Phys. Rev. Lett.* **2005**, *95* (16), 163001.
(41) Tully, J. C. Molecular dynamics with electronic transitions. *J. Chem. Phys.* **1990**, *93* (2), 1061−1071.
(42) Jaeger, H. M.; Fischer, S.; Prezhdo, O. V. Decoherence-induced surface hopping. *J. Chem. Phys.* **2012**, *137* (22), 22A545.
(43) Heyd, J.; Scuseria, G. E. Efficient hybrid density functional calculations in solids: Assessment of the Heyd−Scuseria−Ernzerhof screened Coulomb hybrid functional. *J. Chem. Phys.* **2004**, *121* (3), 1187−1192.
(44) Rudenko, A. N.; Brener, S.; Katsnelson, M. I. Intrinsic Charge Carrier Mobility in Single-Layer Black Phosphorus. *Phys. Rev. Lett.* **2016**, *116* (24), 246401.
(45) Lang, H.; Zhang, S.; Liu, Z. Mobility anisotropy of two-dimensional semiconductors. *Phys. Rev. B: Condens. Matter Mater. Phys.* **2016**, *94* (23), 235306.
(46) Villegas, C. E. P.; Rocha, A. R.; Marini, A. Anomalous Temperature Dependence of the Band Gap in Black Phosphorus. *Nano Lett.* **2016**, *16* (8), 5095−5101.
(47) Abakumov, V.; Perel, V. I.; Yassievich, I. *Nonradiative Recombination in Semiconductors*; Elsevier, 1991.
(48) Zhang, L.; Zheng, Q.; Xie, Y.; Lan, Z.; Prezhdo, O. V.; Saidi, W. A.; Zhao, J. Delocalized impurity phonon induced electron−hole recombination in doped semiconductors. *Nano Lett.* **2018**, *18* (3), 1592−1599.
(49) Chu, W.; Zheng, Q.; Prezhdo, O. V.; Zhao, J.; Saidi, W. A. Low-frequency lattice phonons in halide perovskites explain high defect tolerance toward electron-hole recombination. *Sci. Adv.* **2020**, *6* (7), eaaw7453.
(50) Chu, W.; Saidi, W. A.; Zhao, J.; Prezhdo, O. V. Soft Lattice and Defect Covalency Rationalize Tolerance of β-CsPbI3 Perovskite Solar Cells to Native Defects. *Angew. Chem., Int. Ed.* **2020**, *59* (16), 6435−6441.
(51) Bruzzone, S.; Fiori, G. Ab-initio simulations of deformation potentials and electron mobility in chemically modified graphene and two-dimensional hexagonal boron-nitride. *Appl. Phys. Lett.* **2011**, *99* (22), 222108.
(52) Xi, J.; Long, M.; Tang, L.; Wang, D.; Shuai, Z. First-principles prediction of charge mobility in carbon and organic nanomaterials. *Nanoscale* **2012**, *4* (15), 4348−4369.
(53) Guo, H.; Chu, W.; Zheng, Q.; Zhao, J. Tuning the Carrier Lifetime in Black Phosphorene through Family Atom Doping. *J. Phys. Chem. Lett.* **2020**, *11* (12), 4662−4667.

https://doi.org/10.1021/acs.jpclett.1c00747
J. Phys. Chem. Lett. 2021, 12, 3960−3967